Prediction of thermal crossover based on imaging measurements over the diurnal cycle

Conference Paper *in* Proceedings of SPIE - The International Society for Optical Engineering · August 2003

DOI: 10.1117/12.488358

3 authors, including:

Paul Retief
Incomar Aeronautics
18 PUBLICATIONS **191** CITATIONS

SEE PROFILE

Prediction of thermal crossover based on imaging measurements over the diurnal cycle

S. J. P. Retief, C. J. Willers, M. S. Wheeler

Kentron, Division of Denel, Pretoria, South Africa.

ABSTRACT

Thermal crossover is the phenomenon where the infrared signatures of two different objects in a scene are indistinguishable. A prediction method was developed where a series of infrared images is used as the basis to predict thermal crossover under different climatic conditions. Image recordings are made over the full diurnal cycle, for a fixed scene. We then develop a theoretical thermal model, describing dynamic temporal behaviour. Using the recorded images, the model parameters required to describe the temporal behaviour of the observed scene, are determined. The model, with the appropriate model parameters, is then used to create a new image sequence, predicting the scene appearance under different climatic conditions. The new image sequence is used to predict thermal crossover under the new set of climatic conditions. The paper closes with conclusions and recommendations for future work.

Keywords: Thermal crossover, infrared signature, contrast inversion, low contrast.

1. INTRODUCTION

Thermal crossover is defined[1] as 'a natural phenomenon that normally occurs twice daily when temperature conditions are such that there is a loss of contrast between two adjacent objects on infrared imagery'. To be more precise, thermal crossover occurs when the apparent radiance* contrast between two or more objects in a thermal image is below the threshold value required to execute a specific task.

If the objects have equal emissivities, thermal crossover corresponds to equal temperatures for the objects. Objects with different emissivities would be in thermal crossover at different surface temperatures. When discussing and visualizing thermal crossover, it is convenient to plot temperatures, such as shown in Figure 1. Referring to temperature is a matter of convenience, in reality, radiance from the object's surface is implied.

A means to predict the time period of such thermal crossover occurrences can greatly aid in the planning of commercial tasks or military missions. The success of such a prediction depends on several key factors: (1) the task requirements must be well understood; (2) the terrain characteristics must be known; (3) the sensor's characteristics must be known; and (4) the climatic conditions must be predicted with some accuracy. While the concept of thermal crossover is simple to grasp, attempts at exact mathematical formulation quickly indicate this to be a complex, multi-faceted problem. The complexity of the factors influencing thermal crossover prediction is shown in Figure 2.

A multitude of thermal crossover events take place throughout the diurnal cycle, and it is evident that critical crossover events take place under low light conditions: in the morning and in the evening. The evening crossover consists of a number of discrete crossover events, not all taking place at the same time, because of the objects' thermal history and high contrast conditions. The more important morning crossover occurs after some hours of heat loss during the night, under conditions of low contrast. When observed in different spectral bands, the crossover event will occur at different times. Crossover events should be considered for any system that relies on thermal sensors only.

Kentron, Division of Denel (Pty) Ltd, PO Box 7412, Centurion 0046, South Africa.
E-mail: paul.retief@kentron.co.za, nelis.willers@kentron.co.za, riana.wheeler@kentron.co.za.

*Apparent radiance or radiance contrast is the contrast when viewed at a distance through an intervening and attenuating atmosphere.

Geo-Spatial and Temporal Image and Data Exploitation III, Nickolas L. Faust, William E. Roper, Editors,
Proceedings of SPIE Vol. 5097 (2003) © 2003 SPIE · 0277-786X/03/$15.00

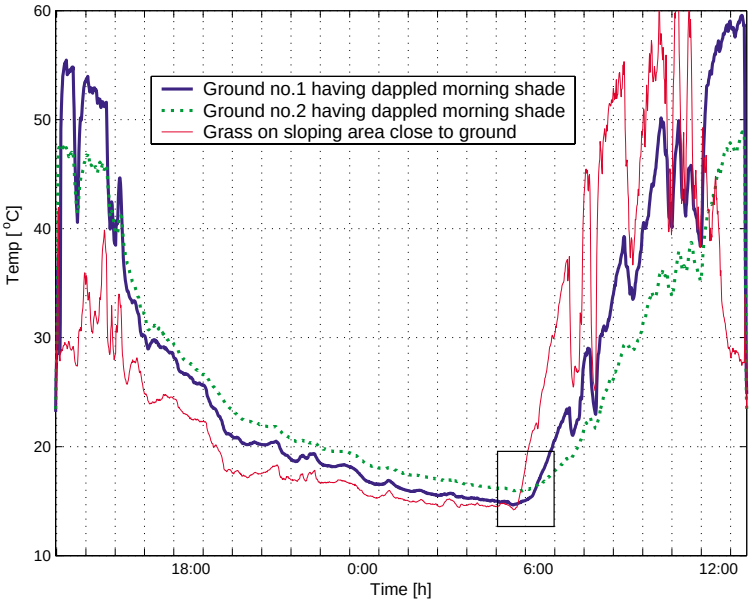

Illustration of thermal crossover: This graph shows grass (lawn) and bare ground micro-thermocouple temperature measurements taken over a 24-hour cycle, on a small patch of uneven terrain. During the day, some measurement points were shaded by trees and/or clouds. The graph clearly shows the cool-down phase during the night, resulting in a low temperature contrast before sunrise. Just prior to the morning crossover, all measurement points were within a range of 3 °C. Temperature crossover events occur throughout the day, but note, in particular, the crossovers in the time period 05:00 to 07:00.

Figure 1. Measured diurnal temperature variations of lawn grass and bare ground on a small patch of uneven terrain

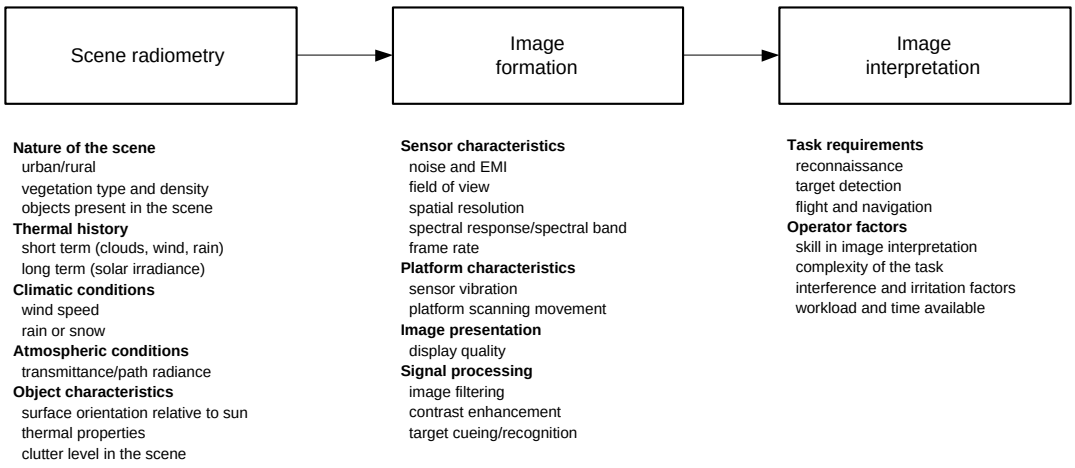

Figure 2. Factors affecting the crossover performance phenomenon

Although the term is commonly used in the military to denote a time duration when some military objective, e.g. safe flying and target recognition, cannot be achieved, very little information on thermal crossover is available in the open literature.

This paper proposes a methodology to facilitate an understanding of the complexities and the interplay between some of the various problem elements. The thesis is that real-world image recordings can be used to extract a thermal scene description, which is used to predict scene appearance under different climatic conditions. The recordings are taken over a 24-hour period at regular intervals. Time domain analysis, which accurately accounts for solar flux and meteorological conditions, renders a series of parameters that describe each pixel in the image as a separate measurement. A previous method[2] is extended by using a more elaborate heat balance model, more data samples and environmental data input, and more sophisticated data analysis.

2. THERMAL CROSSOVER EXPLORED

2.1. Shortcomings of Current Definitions

One definition of thermal crossover is when the temperatures of the target and background are within 2 degrees† of each other.[3] For the purpose of this paper, thermal crossover is considered as a period of time during which a specific task cannot be executed. In the simplest case, the crossover period may have a precise moment of zero contrast, spanned by two periods of 'low contrast'. A scene with a variety of objects and object surface orientations may not have a single moment of crossover, but a number of different crossover events. Furthermore, scene or sensor influences may alter the inherent target contrast, interfering with the perception process. Thermal crossover can therefore be defined as the period of confusion due to insufficient information in the image.

In order to support automated analysis of thermal crossover events, a simplified mathematical norm is proposed for quantifying the information content in the image, relative to the task. Virtually all tasks require the evaluation of a region of interest (ROI) in the image, with the aim of extraction or summarizing the features of relevant objects (targets or background) in the region. Operator tasks can generally be classified into two groups: searching for a specific shape (e.g. target selection and designation) or scene perspective and range determination (e.g. low altitude helicopter flight using thermal imagers). The implications of thermal crossover for these two tasks are significantly different.

2.2. Searching for a Specific Target: Edge Detail

The target search task requires the operator to search the entire image for an object of the expected size and shape. The target is most commonly a man-made object, often recognizable by its shape, texture or internal detail. For this task, thermal crossover can be defined as the time period during which the *specific target* cannot be observed in the image, because *specific features* are not visible. The visibility of specific target features serves as the basis for a method to determine the time duration of thermal crossover.

For the purpose of this paper, an airfield runway's edges were selected to serve as a measure of thermal crossover. The objective is to determine the information missing from the images during crossover, in an image sequence (one minute frame intervals). The Canny edge extraction algorithm[4] was used to extract edges for every image in the sequence. In order to detect the missing edges, an edge map was constructed by applying the logical OR operator to all the edge map images within a predefined time window around the current image. By comparing the edges in the current frame with all possible edges in the window period around the current frame, the missing edges could be detected. The Canny threshold was set quite low, to detect low contrast edges (Matlab[5] code `edge(image1,'canny',[0.002 0.01])`).

For this evaluation, the duration of the reference time window was set to 10 minutes, either side of the current frame. A shorter time period masked some of the crossover events, while a longer time period introduced too many edge details that were not relevant to the current frame. It must be noted that during this 20 minute period, the target contrast was already low. It is quite important that this time window be reasonably short, to capture the edges relevant to the image under consideration. Figure 3 shows sets of three images at different times. The image on the left is the original input image (3–5 μm, simulated), while the centre image shows the edge detail present in a time period around the current frame, but *missing in the current frame* (ignore the right-hand image at this time). The total time during which the overall runway scene (macro scale) did not show sufficient edge detail, was approximately 12 to 15 minutes. Considering only a specific region on the runway (micro-scale), the crossover period was of the order of five to eight minutes.

The objective of this edge detail method is to detect a specific target, against its surroundings. Crossover duration is defined as the time during which missing edges between the target and its surroundings can be detected. The procedure outlined above proved to be easy to calculate. The procedure is quite effective in evaluating the effect of thermal crossover when searching for a target with sufficient edge details. This procedure does not perform well if the scene has less well-defined edges, as will be demonstrated in Section 5.

†It is not clear from the reference whether the 2 degrees criterion refers to degrees Celsius or degrees Fahrenheit.

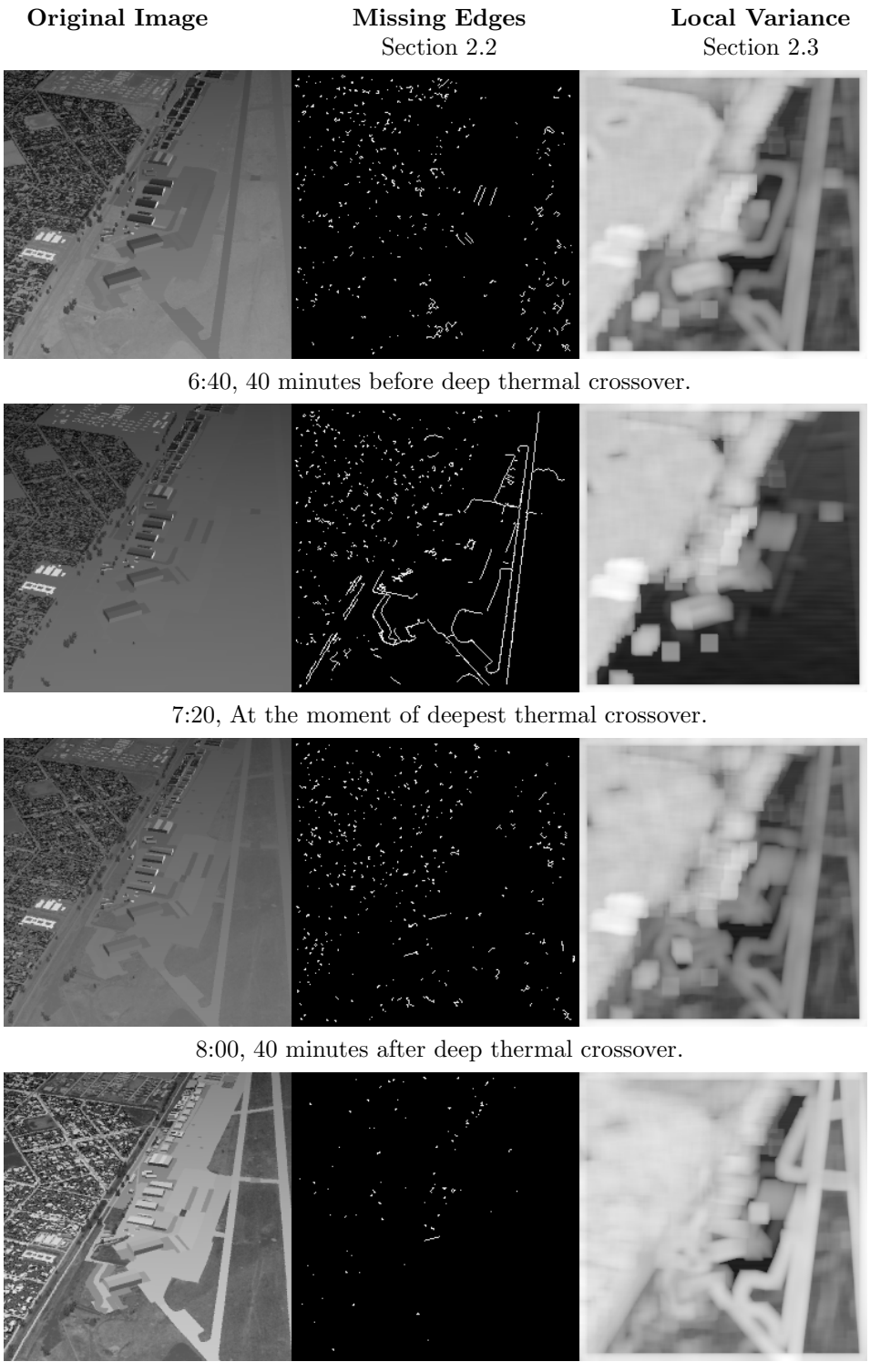

Figure 3. Edge detection during thermal crossover, evaluated on simulation images. The middle image shows edge detail *missing* in the left-hand image, while the right-hand image shows local image variance

2.3. Scene Perspective and Range Determination: Local Variance

When analysing the scene for perspective and range cues, the operator is not searching for a specific target — the operator is searching for anything in the scene that may provide perspective and range information. Firstly, the operator scans the scene, looking for objects that may be used to estimate range to objects in the scene. Often, the object is viewed against other objects of similar size. This leads to the notion of a 'size' within the search region in the image. Secondly, the operator attempts to determine the object features, based on the variation in pixel grey-level values. Note that the operator's ability to extract information from the image is limited by sensor resolution and noise. The required operator model must therefore provide a measure of the information content in the image, relating to objects of a given size.

Define the normalized local variance operator $\mathcal{Q}_{a,b}(I(i,j))$ operating on pixel (i,j) of an image I, by calculating the image grey level variance in a square sub-image of the image spanning columns $[i-a:i+a]$ and rows $[j-b:j+b]$

$$\mathcal{Q}_{a,b}(I(i,j,t)) = \frac{1}{(N-1)}\left[\sum_{p=i-a}^{i+a}\sum_{q=j-b}^{j+b}\left(\bar{I}_{\text{sub}} - I(p,q,t)\right)^2\right], \tag{1}$$

where t is time, N is the number of pixels, and $\bar{I}_{\text{sub}}$ is the average value of image pixels in the sub-image.

The variance of the image sequence $J(i,j,t)$, resulting from the application of the operator $\mathcal{Q}()$ to the image sequence, can be analysed in the time domain to determine the extent of crossover in the input image sequence $I(t)$. For values of $J(t)$ approaching zero, the observed image content is low, either as a result of thermal crossover, or because of low inherent scene contrast. By analysing the temporal response of pixel (i,j) in $J(i,j,t)$, it can be determined whether the scene content is low contrast (small variation), or whether the pixel experienced thermal crossover (larger variation). The time lapse at low values of $J(t)$ provides an indication of the duration of the thermal crossover event.

In this investigation the standard deviation (square root of variance) in the sub-image was used as the operator $\mathcal{Q}()$. Other first-order and second-order statistics, such as entropy,[6] can also be used. The Matlab function `log(nlfilter(imagef,[15 15],'std2'))` was used. This function calculates the standard deviation in a sub-image of 15 × 15 pixels, on a pixel by pixel basis. The resulting images were converted to a video to observe temporal variations. Extracts from this video are shown in Figure 3. The image on the right shows the local standard deviation in the input image. The crossover duration was of the order of five to 10 minutes. The video shows that the time duration of a deep crossover, as defined by local variance, is at most two to three minutes long.

The local variance procedure outlined above requires an intensive calculation, but it serves reasonably well to determine the image content for the purpose of crossover evaluation.

3. METHODOLOGY FOR CROSSOVER SIMULATION

3.1. Thermal Equilibrium and Data Required

In principle, it is possible to extract an object's thermal parameters if the object's temperature is known under the influence of known environmental conditions. These conditions must be specified in terms of the heat exchange mechanisms between the object and all other interacting elements in the environment. The object can be considered in instantaneous thermal equilibrium with its environment, provided that any change in the environmental conditions is immediately reflected in the objects temperature. Thermal equilibrium conditions in nature will only be fulfilled whenever no 'strong' temporal gradients exist. Any steep gradients in environmental conditions will cause a non-zero net heat flow between the environment and the object, resulting in a change in the object's thermal state. Under transient conditions, the heat flow between the object and the environment is not really in perfect balance (i.e. not a zero net heat flow). The degree of imbalance will be proportional to the temporal gradient in the system.

Despite the limitations brought about by the assumption of thermal equilibrium, the heat balance equation presents a suitable statement of heat exchange between the object and its environment. The solution to the heat balance equation provides a means to obtain the object's thermal parameters. In order to solve the object's

thermal parameters from a number of unique environmental observations, at least as many unique observations are required as there are unknown parameters, i.e. the problem statement must not be under-determined. If more unique observations are available (over-determined system), the solution will provide a 'best fit' of the object's thermal parameters. In this instance the requirement for a well-determined system can be met by a sufficient number of samples.

A previous investigation[2] followed the concept stated above by using the temperatures obtained from two infrared image measurements for the case when the heat exchange mechanisms of radiation (absorption of sun radiation and emission due to own temperature) and heat conductivity (between object and underground thermal bath) are considered. This method is expanded here, by the introduction of additional environmental and object thermal parameters. However, to solve such an expanded heat balance equation, the number of unique recordings must also increase, as mentioned previously.

3.2. Heat Balance Equation

A simplified heat balance equation is used to model the thermal behaviour of an object. The model includes (in the order shown in Equation 2) (1) solar irradiance; (2) ambient irradiance; (3) self emittance; (4) heat conduction to an inner thermal mass; (5) convection heat loss; (6) a correction factor to account for transient heat flow. An evaporation term was also originally included, but the added complexity did not warrant the benefit. The individual terms have simple, non-spectral forms — attempting to solve the heat balance equation when the terms are spectrally formulated, will increase the computation time substantially. During the transient conditions of thermal crossover, there is no thermal equilibrium between the object and its environment, and it is necessary to include the correction factor, here denoted by Φ. The heat balance equation, based on previous work,[7] is modified as follows:

$$\begin{aligned} r \;=\; & +\alpha_s E_s(t_i)\left(\cos\beta(t_i)\sin\gamma(t_i)\cos\zeta\sin\psi+\cos\beta(t_i)\cos\gamma(t_i)\cos\zeta\cos\psi+\sin\beta(t_i)\sin\zeta\right)/\sin\beta(t_i) \\ & +\alpha_l E_l(t_i) \\ & -\epsilon\sigma T_s^4(t_i) \\ & -H\left(T_s - T_{in}\right) \\ & -\left(1.7|T_s(t_i)-T_{amb}(t_i)|^{1/3}+\frac{6V^{0.8}(t_i)}{D^{0.2}}\right)\left(T_s(t_i)-T_{amb}(t_i)\right) \\ & -\Phi, \end{aligned} \tag{2}$$

with parameters defined in Table 1. The heat balance equation applies at all times t_i.

The fourth term in Equation 2 assumes that each object can be modelled by an outer surface connected to a constant temperature (T_{in}) inner heat reservoir. A single valued heat conductance H applies between the surface and the inner reservoir. This approach is not used in the original model.[7] Although the model defined in Equation 2 applies reasonably well to macro-scale objects, it is not accurate for smaller objects, with small thermal inertia. An object with small thermal inertia, thermally isolated from surrounding objects, such as a metal roof, a rock, grass or leaves, should be modelled as a solid uniform object, instead of an internal source conducting to the outer surface.

While the heat balance equation is normally applied to an object as a whole, the method proposed here applies the heat balance equation to individual pixels in the image, as if each pixel is an object on its own.

3.3. Experimental Field Work

Data were recorded using a number of instruments, including a 3–5 μm thermal imager (CEDIP Jade3 MWIR), and a weather station recording atmospheric pressure, average wind speed and direction, relative humidity, ambient temperature and solar irradiance in the 0.3–3 μm spectral band. The equipment was situated on a platform approximately 5 m above ground level, looking down on a scene consisting of patches of open soil, tall grass, rocks, bushes, trees and the horizon in the distance. The distance to the objects of interest ranged from 30 m to 50 m, partially obviating the need to account for atmospheric transmittance.

Table 1. Parameters in the heat balance equation

Measured and calculated input parameters	
E_s	Solar irradiance, 0,2–3 μm spectral band [W/m^2]
E_l	Atmospheric and ambient irradiance, calculated[8] from ambient temperature and partial water pressure with $E_l = \sigma T_{amb}^4(t_i)\left(0.605 + 0.048\sqrt{P_p(t_i)}\right)$
β	Sun elevation, calculated by computer program
γ	Sun azimuth, calculated by computer program
T_{amb}	Ambient temperature [K], measured
V	Wind velocity [m/s], measured
P_p	Water partial pressure in [mbar], derived from humidity measurement
T_s	Object surface temperature [K], thermal imager measurement
Parameters to be solved	
α_s	Effective solar absorptivity (0.2–3 μm spectral band) [-]
α_l	Effective ambient absorptivity (3–12 μm spectral band) [-]
ϵ	Effective emissivity [-]
T_{in}	Object internal temperature [K]
H	The conductive heat transfer coefficient between the object surface and its internal core [W/m^{2}K]
D	The surface's characteristic lateral dimension [m]
ψ	The object's surface normal vector elevation angle
ζ	The object's surface normal vector azimuth angle
Φ	Correction factor to account for transient conditions heat flow [W/m^2]
Other constants	
σ	5.67×10^{-8} Stefan-Boltzman constant [W/m^{2}K^4]
r	Residual to be minimized $r \to 0$

Recordings were made facing to the north, in late summer, in Pretoria (25°55′S 28°11′E, altitude 1350 m above sea level) over a 24-hour period. During the recording period, clouds were present intermittently. The image recordings were made at one-minute intervals over the full recording period. Figure 4 shows the scene in the visual and thermal spectral bands. Figure 5 shows a time sequence of peak normalized environmental input parameters during the test.

The observed temperature measurement with the 3–5 μm thermal imager is affected by the presence of reflected sunlight. In subsequent work, the contribution of reflected sunlight to the temperature measurement will be corrected. Alternatively, an 8–12 μm thermal imager can be used.

For the purpose of surface temperature measurement with the thermal imager, the object emissivity was assumed to be unity.

Figure 6(a) shows the minimum, 1-percentile, median, 99-percentile and maximum observed temperatures in the selected image subset as a function of time. Similar plots for the whole scene indicate that different percentile levels in the image start to increase at slightly different times. The temperature increase at lower percentile levels lags the increase at higher percentile levels by approximately 15 minutes (not visible in Figure 6, since these plots apply to a small sub-image).

Retrospectively, it is clear that the scene, at relatively short range, had too much micro-detail. The convective cooling caused by the wind gusts also resulted in a random noise effect in the image, effectively hiding any subtle crossover effects that may have been present.

(a) (b)

Figure 4. Field trial scene, (a) visual and (b) thermal images, showing the region used in this investigation

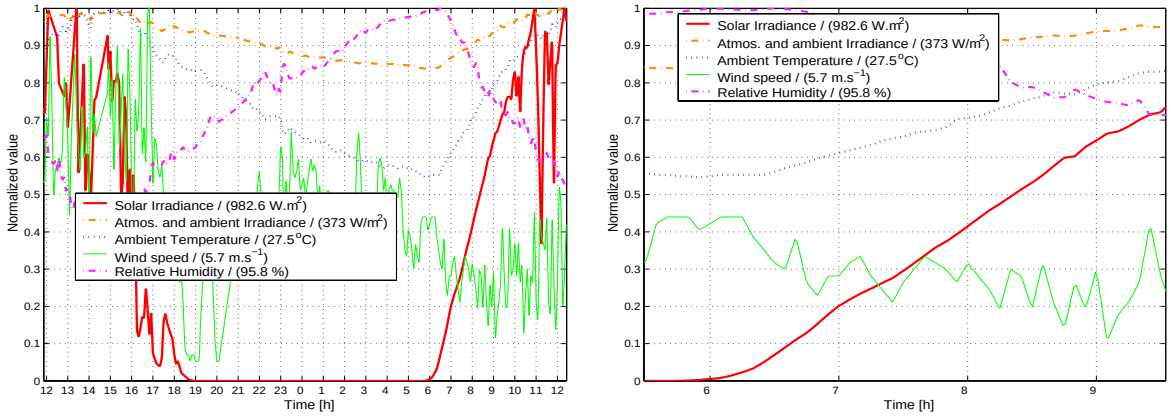

(a) (b)

Figure 5. Environmental conditions/parameters on the day of the test, all data peak normalized to unity. Normalizing factors are shown in brackets. (a) covers the full diurnal cycle, while (b) covers only the crossover period

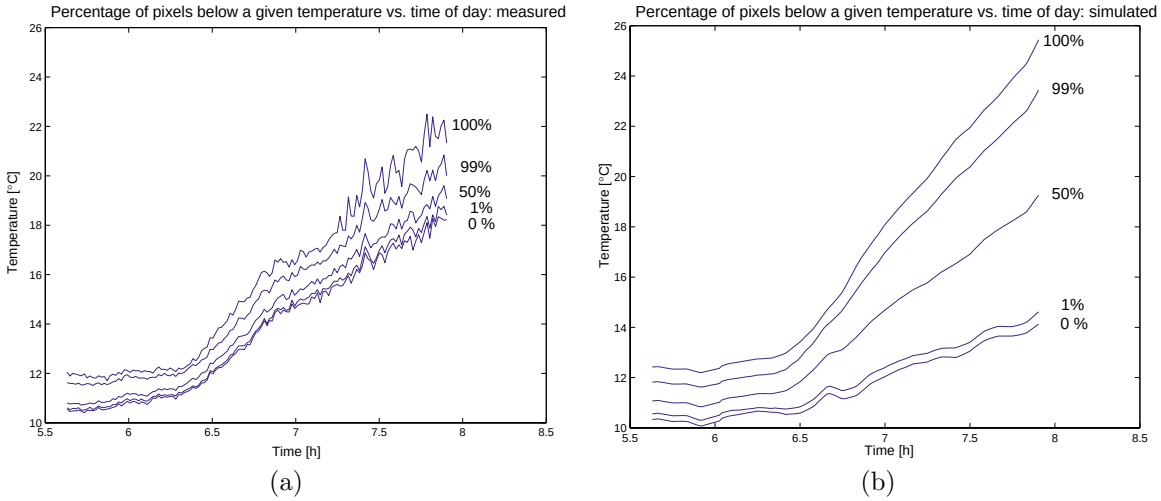

(a) (b)

Figure 6. Pixel statistics in the sub-image at a given temperature, as a function of time of day: (a) measured and (b) simulated

4. DATA REDUCTION AND PARAMETER ESTIMATION

The scene recorded during the field trial did not show thermal crossover on a macro scale. The best crossover event was between a rock and its surroundings, in the upper central region of the image, indicated by the block (35 × 47 pixels) in Figure 4. This block was selected for further processing and analysis. The temperature difference between the rock and the grass was less than 1 °C, gradually diminishing to zero difference, as the temperatures of both rose by approximately 7–8 °C.

The heat balance equation was solved for each pixel in the selected block, finding the minimum residual r over the sequential samples, collectively. This means that the parameters are considered constant over the full sampled period (135 minutes for this investigation). The parameters obtained by this solution were used to simulate new images, using the same environmental parameters as well as using new environmental parameters.

Thermal crossover is a dynamic process, and is not easily observed or documented in still images. During the course of the investigation image sequences were converted to video form to study the dynamic nature of the scene changes. Quite often, effects not evident in still images became observable in the dynamic image sequence displays.

Equation 2 contains a number of known parameters (by measurement or prediction) and a number of unknown parameters, to be solved by minimization. Considering the number of parameters to be solved, Table 1, it is evident that the high dimensionality of the problem presents formidable challenges. Initial experiments indicated the difficulty of minimizing this multi-dimensional problem: a large number of possible solutions exist, most of which had no physical significance (e.g. complex emissivity, negative absolute internal temperature). Conventional unconstrained minimization techniques (Matlab `nlinfit`) did not yield physically feasible solutions. Since one of the objectives is to apply the model with different input parameters, it is imperative that the solution be reasonable in a physical sense. The application of Monte Carlo techniques, in conjunction with tightly constrained parameters, provided physically feasible results, albeit at increased computational load. The constraints were selected to be reasonable in a real world physical sense .

When analysing the early morning crossover, there appears to be a reasonable convergence on some of the parameters (α_l, ϵ, T_{in}, H, Φ). Other parameters (α_s, ζ, ψ, D) do not exhibit well-behaved convergence — and most of these are related to solar heat influx. This lack of convergence is a cause of concern, since the solar flux plays a key role in the early morning crossover. The lack of convergence could be partly ascribed to the complexity of performing accurate solar flux measurements in the early morning, before and during sunrise.

Convective wind cooling played a prominent role, even at the relatively low wind speeds experienced during the recordings (2.5 m/s average, 5.7 m/s maximum). This effect is readily observed, when playing the infrared video sequence, as a near-random variation in image gray level of objects with low thermal inertia. The directional cooling of tufts of grass clearly shows the direction of irregular wind gusts, and the temperature variation indicates wind speed. Objects with higher thermal inertia are less affected by wind gusts.

The continual variation in wind speed resulted in variations in surface temperature, especially on surfaces with low thermal inertia (e.g. grass, which dominated the test scene). These variations play havoc with the data reduction process, by introducing noise into the input data. The solver seems to eliminate the wind-induced noise by requiring the D factor to be very high, thereby minimizing the effect of wind speed on the solution. In follow-up work, the short term variation in wind speed will be removed prior to solving the heat balance equation.

The inability of the heat balance equation (Equation 2) to account for all observed phenomena, sets a limit on the modelling accuracy. To improve the quality of the simulated images, the heat balance equation must be reviewed and expanded.

Table 1 parameters, displayed in the form of images, did not show any spatial resemblance to the original input image. The solutions for respective pixels are therefore completely uncorrelated. If the solver can be constructed to be sensitive to surrounding pixels, the parameter images should resemble the structure of the input image.

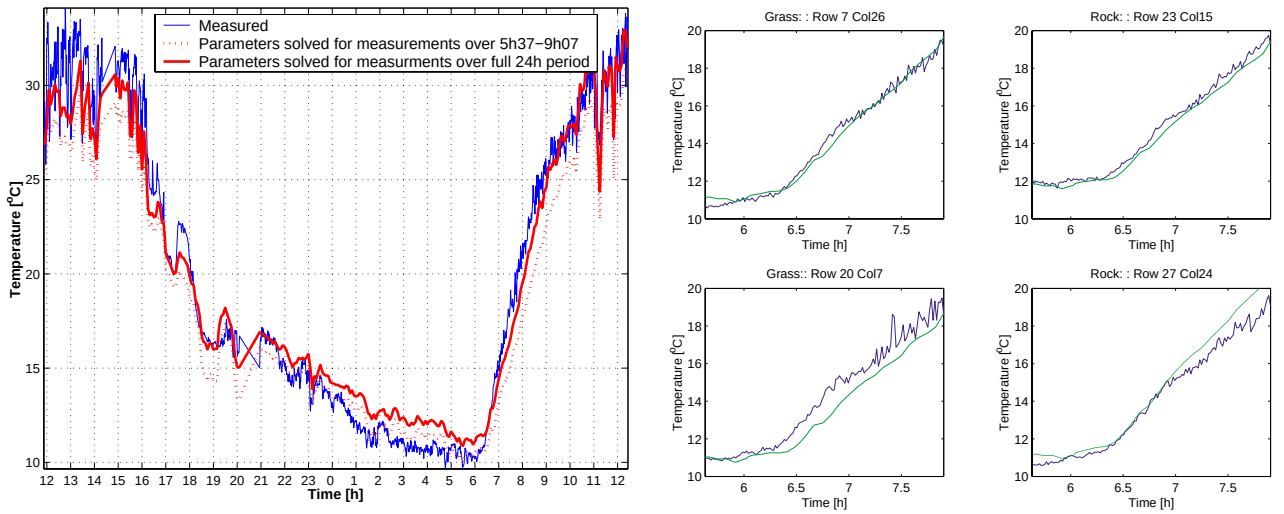

(a) (b)

Figure 7. Comparison of simulated and measured diurnal surface temperature variations for a single pixel: (a) diurnal cycle, (b) crossover period (jagged lines are measured data and smooth lines are simulated data)

5. THERMAL MODELLING AND CROSSOVER PREDICTION

After solving for the pixel parameters, the heat balance equation was applied to create images of surface temperature T_s, given a set of meteorological data. If the solution is correct, the simulated images and the original recorded images should be similar. During initial experiments we allowed a relatively large residual error, and the synthetic image quality was poor. Lowering the allowable residual error resulted in improved image quality, but also in exponentially longer execution times. Specific pixels proved to be 'problem pixels,' consistently resisting solution, having higher solution residues and poorer performance than the 'well-behaving' pixels.

Figure 7 shows a comparison of the measured temperatures and the simulated surface temperatures, for selected pixels. Figure 7(a) shows the comparison of predictions made with parameters solved over the full diurnal cycle, and parameters solved over the crossover period only. Figure 7(b) provides comparisons for four different pixels with parameters solved over the crossover period. The smoother lines were calculated with the model, and the field trial measurements show mode jagged lines because of wind speed variations. The results shown in Figure 7(b) correspond with the images shown in the first and second columns of Figure 8.

When solving for parameters over a limited time period only (Figure 7(b)), the simulated temperature is mostly within 1–2 °C of the measured temperature. This error would appear acceptable, but considering the objective to create images to predict thermal crossover, this performance might not be good enough. These temperature errors manifest itself in the image as noise, caused by the uncorrelated solutions of adjacent pixels. The noise results in poor outlier statistics performance, as can be seen in Figures 6 and 8. The statistical spread in the simulated images far exceeds the spread observed in the real image. Further work is required to resolve this issue.

Figure 8 shows real and simulated images before and during crossover. The columns in this figure show the original input image, a simulated image corresponding to the trial conditions, another simulated image with different environmental conditions, the Section 2.2 edge measure with `edge(b,'canny',[0.01 0.02])` processing of the original image, and the Section 2.3 variance measure (7×7 pixel block size) of the original image. Each row in the grid of images represents a different moment in time, and the median temperature T_m and 1-percentile to 99-percentile temperature ranges ΔT are stated below each image.

One of the requirements of this experimental concept is spatial fidelity; that the solutions of all pixels belonging to one object in the image should be reasonably convergent on key parameters (i.e. internal temperature). This objective is not achieved when each pixel in the image is solved independently of its neighbours. The ideal solver

must therefore find a two-dimensional, localized Monte Carlo solution, cognizant of the image/scene contents. The automatic correlation of pixel type could possibly be done using neural networks or similar techniques.

One of the objectives with the investigation was to use the trial data to predict crossover under different conditions (e.g. another time of year). The parameters determined for the trial conditions, were used to predict new surface temperatures T_s, with new environmental conditions. Figure 8 shows the results obtained for a 7 °C ambient temperature T_{amb} increase (with a concomitant increase in ambient irradiance E_l) and the solar irradiance E_s was increased by 2 %. The internal temperature T_{in} was also increased by 7 °C, following the increase in ambient temperature. The results (middle column of Figure 8) demonstrated that the model can be used with different environmental data, to yield new image sequences.

Experiments indicated that the edge map analysis is less well suited to smaller images, and is furthermore affected by noise in the image as caused by the semi-random wind cooling in this case. The variance map analysis performed better, but is sensitive to single pixel targets (see the central top part of the image).

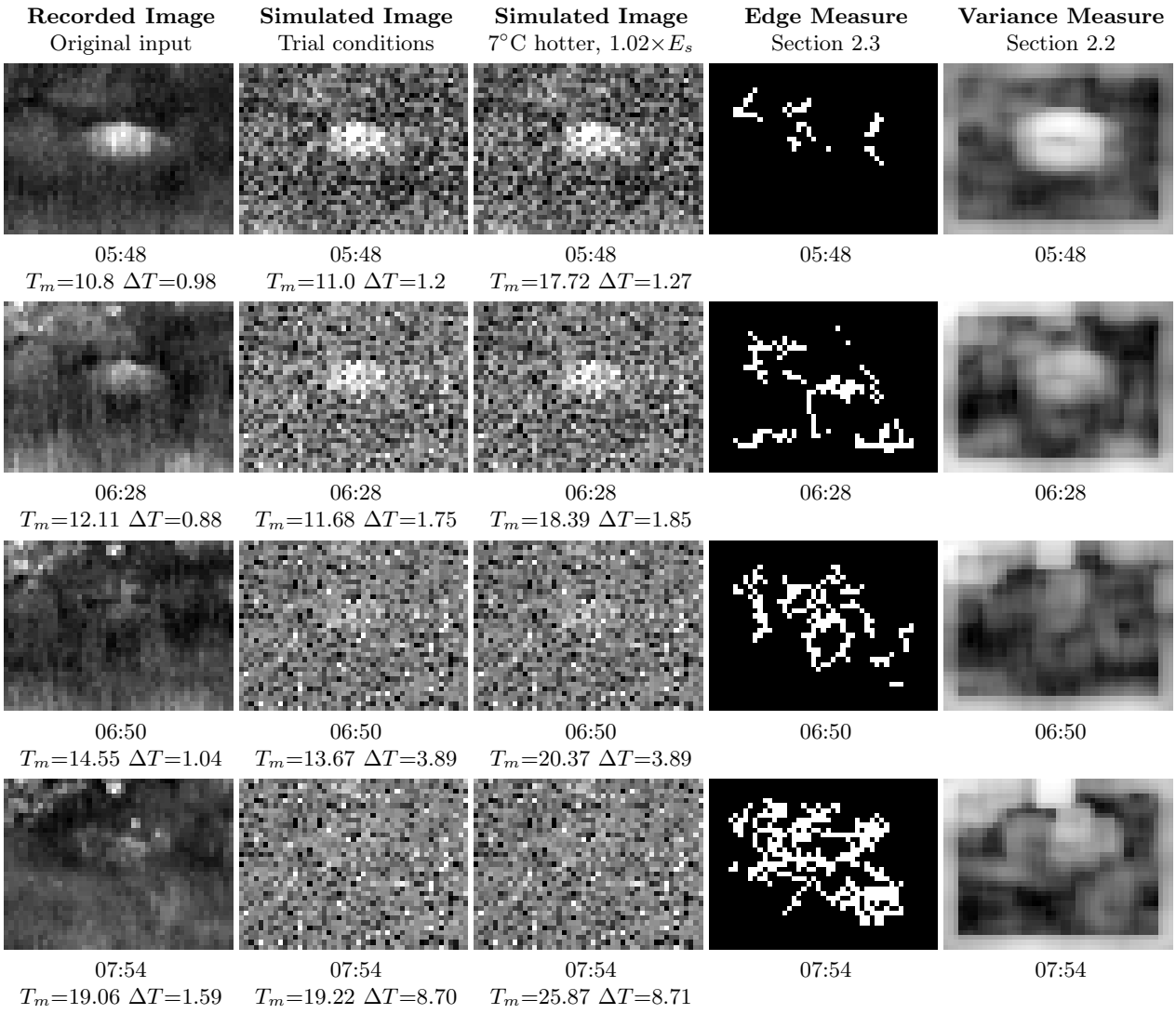

Figure 8. Recorded and simulated images at different times of day

6. CONCLUSION AND RECOMMENDATIONS

The application of the heat equation to pixel-scale elements appears to to be suitable for the prediction of thermal crossover. It is evident that some parameters should be considered as time varying. This requirement depends on the nature of the object. Objects with *low thermal inertia*, such as grass or leaves, require time varying internal temperature, while objects with *large thermal inertia* could be modelled by fixed parameters.

A number of key issues are now clear: (1) thermal crossover is best observed and analysed on a macro-scale; (2) not all scenes will always exhibit thermal crossover — factors such as the distance to the scene, viewing angle (depression angle), diversity of objects, and variation in thermal properties, affect the probability of occurrence and the degree of crossover; (3) a complex scene will almost always have some regions with high contrast, whereas a simple scene (e.g. sandy desert) may have more pronounced crossover; (4) not all thermal crossover events take place at the same moment in time — in a complex scene, there would always be regions with non-zero contrast.

The accuracy of the method used in this investigation, is affected by a number of factors: (1) influence of sun reflection in the 3–5 μm spectral band; (2) lack of atmospheric transmittance correction; (3) constraints placed on the solution; (4) poor correlation between solutions for adjacent pixels in the image; (5) the lack of spectrally accurate calculations; (6) the sufficiency of the heat balance equation to account for all physical effects; (7) value of the emissivity used for temperature measurement by a thermal imager. All these factors can be addressed in a more comprehensive solution.

This investigation has shown that it is feasible to create simulated images corresponding to different environmental conditions, using a well-instrumented trial as input. If the objective of accurately predicting thermal crossover is to be met, several improvements to the current process would be required. These improvements should be possible, and the end objective of predicting thermal crossover is feasible.

ACKNOWLEDGMENTS

We gratefully acknowledge Bernard Willers and Denise Ansell's review of this paper.
The execution of this work was funded by the Kenis Thermal Imager Programme, Kentron, Division of Denel, South Africa.

REFERENCES

1. http://www.dtic.mil/doctrine/jel/doddict/data/t/05310.html
2. N. Ben-Yosef, S. Lashansky, K. Wilner, M. Abitbol, 'Temporal prediction of infrared images of ground terrain', *Applied Optics*, **26**, pp. 2128–2130.
3. D. L. Martens, 'Communicating the Weather: The Garske Chart', in *Military Intelligence Professional Bulletin*, http://www.fas.org/irp/agency/army/tradoc/usaic/mipb/1998-1/MARTfnl.htm.
4. J. Canny, 'A Computational Approach to Edge Detection', *IEEE Transactions on Pattern Analysis and Machine Intelligence*, **8**, Nov. 1986.
5. Matlab 6, Release 12.1 includes a function `edge` that provides a number of different edge extraction algorithms. The MathWorks, Inc., 3 Apple Hill Drive, Natick, MA 01760-2098.
6. S. Theodorides, K. Koutroumbas, 'Pattern Recognition', ISBN 0-12-686140-4, Academic Press, 1999.
7. D. Kryskowski, G. H. Suits, 'Natural Sources', in *The Infrared and Electro-Optical Systems Handbook: Sources of Radiation*, F. G. Smith, ed., pp. 145–151, SPIE Optical Engineering Press, Bellingham, 1993.
8. D. Kryskowski, G. H. Suits, 'Natural Sources', in *The Infrared and Electro-Optical Systems Handbook: Sources of Radiation*, F. G. Smith, ed., Equation 3.14, p. 147, SPIE Optical Engineering Press, Bellingham, 1993.